Dynamics of low-energy holes in germanium

Rainer Till and Fritz Keilmann

Max-Planck-Institut für Festkörperforschung, 7000 Stuttgart 80, Federal Republic of Germany

(Received 27 November 1990)

We study inter- and intra-valence-band relaxation of germanium, both experimentally and theoretically, by saturation spectroscopy. Far-infrared laser pulses with intensities between 1 and 10^5 W/cm^2 are applied to saturate direct heavy-hole-to-light-hole transitions. The characteristic saturation intensity I_s is measured for a range of frequencies (28–174 cm^{-1}) and temperatures (20–100 K) and found to vary over two orders of magnitude: I_s increases approximately linearly with frequency; a minimum is observed at 30 K. This complex behavior is consistent with a model of inhomogeneously broadened two-level systems that takes explicit account of, and thus quantifies, the various scattering contributions from phonons, impurities, and holes. The theory predicts a saturation-induced dip in the absorption spectrum, which is also experimentally observed and yields the dynamical time constants $T_1 = 43$ ps and $T_2 = 1.5$ ps, for energy and phase relaxation, respectively, at 31.2 cm^{-1} and 40 K.

I. INTRODUCTION

The scattering of mobile charge carriers is fundamental to electronics, yet the usual transport methods measure only the average scattering of many states; state-selective scattering experiments are therefore highly desirable. We discuss the use of the valence bands (of Ge) where optical pumping with *far-infrared* radiation can selectively populate low-energy states of mobile holes, the scattering of which can be determined by the effect of absorption saturation. Note that no extra electron-hole pairs are produced, which is a great advantage over the common optical pumping at near-visible frequency.

The *mid-infrared* (≈ 1000 cm^{-1}) absorption due to transitions between the heavy- and light-hole valence bands in germanium is saturable at room temperature[1–3] and also at liquid-nitrogen temperature.[4] All authors find that the absorption coefficient α depends on intensity I according to

$$\alpha \approx (1 + I/I_s)^{-x} , \qquad (1)$$

with a saturation intensity I_s, but disagree on the exponent of either $x = 1$ (Refs. 1 and 4) or $x = 0.5$ (Refs. 2 and 3). The latter is theoretically expected from applying the model of inhomogeneously broadened two-level systems to the valence bands where optical-phonon scattering dominates the relaxation.[2] This model is convincing by its simplicity and gives the same intensity dependence of the absorption coefficient as a rigorous theoretical treatment.[5] It allows us to derive the product of energy and phase relaxation times just from a measurement of the saturation intensity. It also predicts the appearance of a saturation dip in the spectrum, a phenomenon well known in the spectroscopy of molecules and atoms, from which both dynamical times can be separately determined.[6] This dip was indeed observed in *p*-type Ge, in good agreement with the predictions of the model.[7]

A different regime of relaxation is expected for holes of low energy $E_h \ll E_{op}$, where $E_{op} = 300$ cm^{-1} is the energy of an optical phonon. *Far-infrared* light can excite holes to these low energies, and optically pumped gas lasers powerful enough to investigate nonlinear absorption are available.[8] A lower-energy limit of holes that can be studied selectively is posed by $E_h \leq \hbar/\tau$, where τ is the scattering time, since the laser-induced resonance becomes overdamped.

Current interest in the far-infrared spectroscopy of *p*-type Ge is further spurred by the discovery of inter-valence-band lasing. In the *p*-type Ge laser, mutually orthogonal electric and magnetic pump fields achieve a population inversion between light and heavy holes at low temperature.[9,10] The broad spectral region of inversion should allow tuning of the frequency by an order of magnitude. Therefore this laser is expected to be a unique, coherent, and powerful source in the far infrared. Of course, the operation of the *p*-type Ge laser is sensitively influenced by the dynamics of scattering in the valence bands. Our present study of the hole dynamics of *passive p*-type Ge material can serve as the basis for a future theoretical modeling of the *p*-Ge laser.

We begin in Sec. II with an investigation of the absorption of *p*-type Ge at low temperatures. Regions in temperature and frequency space are identified in which the interband transitions dominate the absorption and thus can be selectively studied by nonlinear spectroscopy.

In Sec. III we present the model of inhomogeneously broadened two-level systems applied to the valence bands of *p*-type Ge. We demonstrate that the model explains small-signal inter-valence-band absorption spectra. A discussion of the various scattering mechanisms for holes in *p*-type Ge follows. Theoretical rates for the scattering of holes from phonons, impurities, and holes are used to calculate the energy and phase relaxation times. With these we are able to predict the saturation intensity I_s versus temperature and frequency.

In Sec. IV we describe the saturation experiments. Care is devoted to obtain an absolute intensity scale. The results are discussed and found to agree with the model

of inhomogeneously broadened two-level systems. They are at variance, however, with a model presented by Beregulin et al.[11] which assumes that the bleaching is due to a heating of the hole gas.

Finally, we present in Sec. V a pump-and-probe experiment that reveals a saturation dip in the inter-valence-band absorption in the far infrared. From the width of this dip and the saturation intensity, we calculate both dynamical time constants separately, and obtain agreement with the saturation data. The existence of the saturation dip is a direct proof of the state selectivity of the method.

II. SMALL-SIGNAL ABSORPTION IN THE FAR INFRARED

There are four different ways for a far-infrared photon to become absorbed in p-type Ge.

(1) Interband: Free holes can undergo direct transitions between the heavy- and light-hole valence bands. This interband absorption was first calculated by Kahn[12] under the approximation of a parabolic and isotropic band structure. His results are identical with those obtained by Murzin[13] when the free parameter of Kahn is set to

$$A_{12} = \frac{m_0}{\sqrt{8}} (1/m_2 + 1/m_1) = 7.2 , \qquad (2)$$

as is proposed by Rebane.[14] In the above expression, m_0 is the free-electron mass and m_1 and m_2 are the effective masses of heavy ($m_1 = 0.35m_0$) and light holes ($m_2 = 0.043m_0$), respectively.

The only author to include the full band structure in the calculation of inter-valence-band absorption is Rebane,[14] but his results are only applicable to higher and lower frequencies than those of interest here. So we use the expression of Murzin.[13] The resulting rather flat spectrum for a temperature of 40 K and an acceptor concentration of 4.4×10^{14} cm^{-3} is plotted in Fig. 1 (curve 2); the shape of this function is mainly given by the distribution of heavy holes versus energy. The absorption has a maximum at about 30–40 K (Fig. 2), depending on the frequency, since at low temperatures the holes freeze out, while at high temperatures they spread out over a large energy range. Figure 1 further shows the experimental absorption spectrum of Ge:Ga ($N_A = 4.4 \times 10^{14}$ cm^{-3}), taken at a temperature of 40 K with a Fourier spectrometer (Bruker model IFS 113 v).

(2) Drude: Free holes can make intraband transitions by interaction with a phonon (Drude absorption). This absorption, calculated after Seitz,[15] is significant only at very low frequencies or high temperatures (Figs. 1 and 2).

(3) Impurity: Shallow impurities (gallium atoms in our example) absorb by excitation into discrete levels, which results in sharp structures in the frequency region between 50 and 80 cm^{-1} (Fig. 1).[16] When the photon exceeds the ionization energy (11.3 meV or 91 cm^{-1}), ionizing transitions into the continuum of valence-band states occur. The absorption coefficient due to ionization of impurities is calculated according to Ref. 17. As shown in Figs. 1 and 2, it can be quite large at low temperatures, while it decreases at higher temperatures,
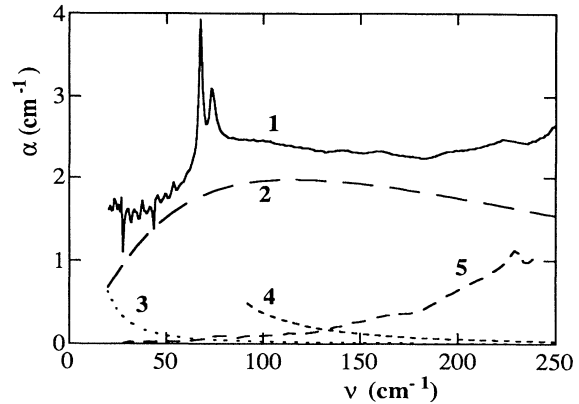

FIG. 1. Far-infrared absorption of Ga-doped germanium, with $N_A = 4.4 \times 10^{14}$ cm^{-3} at 40 K. 1, experimental Fourier spectrum; 2, calculated interband absorption; 3, calculated Drude absorption; 4, calculated absorption due to ionization of impurities; 5, experimental Fourier spectrum of *high-purity* Ge.
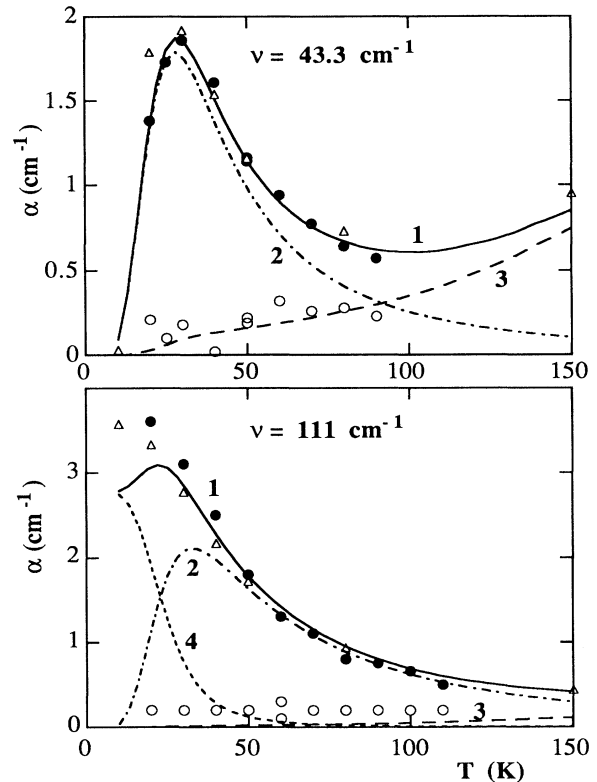

FIG. 2. Electronic part of absorption vs temperature, with $N_A = 4.4 \times 10^{14}$ cm^{-3}. Solid circles, laser measurements; open triangles, Fourier measurements; open circles, residual (not saturable) absorption from high-intensity laser measurements. 1, calculated total absorption; 2, calculated interband absorption; 3, calculated Drude absorption; 4, calculated absorption due to ionization of impurities.

where the impurities become thermally ionized.

(4) *Lattice: Finally, far-infrared radiation interacts with the lattice.* Two-phonon difference processes are relevant in the frequency and temperature range of interest.[18] The lattice absorption is, however, small,[18,19] as is also verified by a measurement of the absorption of an undoped ultrapure sample with an impurity concentration of less than 10^{10} cm^{-3} (Fig. 1).

We see that the experimental spectrum (Fig. 1) is well explained by the sum of the different contributions. This remains true for temperatures in the range 10–150 K and frequencies of 43.3 and 111 cm^{-1} (Fig. 2). Good agreement is found between Fourier and laser measurements (Fig. 2).

For our study of carrier dynamics, we are interested in obtaining the nonlinear intensity dependence of the interband excitation selectively. Therefore we choose the frequencies to lie away from the lines of impurity absorption. In the high-frequency range, where the ionization of impurities is unavoidable, we have to keep in mind that below 40 K a significant part of the absorption is due to impurity absorption.

III. THEORY OF ABSORPTION SATURATION

The valence bands in p-type Ge were treated by a model of inhomogeneously broadened two-level systems to explain the saturation behavior of the inter-valence-band absorption at CO_2-laser frequencies.[2,7] We use a similar model here. In a direct transition the heavy-hole state represents the lower state (1) and the light-hole state the upper state (2), respectively (Fig. 3). The absorption coefficient α for a (homogeneous) two-level system is[20]

$$\alpha(\Omega\omega) = \frac{\pi L \Omega}{\eta c \hbar \epsilon_0} \frac{|\mu|^2}{3} (N_1 - N_2) g_L(\Omega, \omega) , \quad (3)$$

where ω is the frequency and $\Omega = (\epsilon_2 - \epsilon_1)/\hbar$ is the resonance frequency of two-level systems with energies ϵ_1 and
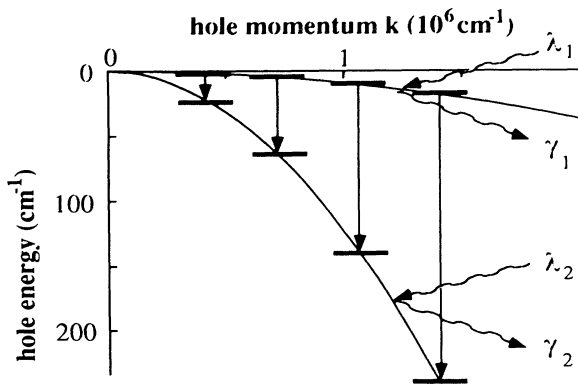

FIG. 3. Valence bands of p-type germanium modeled as inhomogeneously broadened two-level systems. The straight arrows correspond to optical excitation; γ_i and λ_i are the nonradiative excitation and deexcitation rates, respectively.

ϵ_2. L is the Lorentz factor, which equals 1 for delocalized carriers,[20] $\eta = 4$ is the refractive index of Ge, c is the vacuum speed of light, ϵ_0 is the dielectric permeability of the vacuum, μ represents the dipole matrix element connecting the upper and lower states, and N_1 and N_2 are the densities of two-level systems in the lower and upper states, respectively. g_L is given by the Lorentzian lineshape function

$$g_L(\Omega, \omega) = \{\pi T_2[(\Omega - \omega)^2 - 1/T_2^2]\}^{-1} , \quad (4)$$

where T_2 is the phase relaxation time that defines the homogeneous linewidth of the transition.

Since the energy difference between heavy- and light-hole bands varies as a function of quasimomentum k, the resonance frequencies of individual two-level systems vary, similar to the variation of resonance frequencies due to the Doppler effect in the spectroscopy of atoms and molecules. To calculate the absorption coefficient in this case, one has to integrate Eq. (3) over all resonance frequencies Ω,

$$\alpha(\omega) = \int_0^\infty \alpha(\Omega, \omega) g_D(\Omega) d\Omega . \quad (5)$$

In the limit of dominantly inhomogeneous broadening, the homogeneous linewidth $\Delta\omega_0 = 2/T_2$ of the individual systems is negligible compared to the range of resonance frequencies $g_D(\Omega)$, and thus the integration yields

$$\alpha(\omega) = \frac{\pi L \omega}{\eta c \hbar \epsilon_0} \frac{|\mu(\omega)|^2}{3} \Delta N(\omega) g_D(\omega) . \quad (6)$$

We use the approximation of parabolic, spherically symmetric bands so that the population difference $\Delta N = N_1 - N_2$ and the distribution g_D are functions of energy only. Assuming a thermal distribution of carriers $f(\epsilon)$, a density of states $D(\epsilon)$, and a density n of carriers in the valence bands, we obtain

$$\alpha(\omega) = \frac{\pi L \omega n}{\eta c \epsilon_0 (1/m_2 - 1/m_1)}$$
$$\times \frac{|\mu|^2}{3} \left[\frac{D(\epsilon_1) f(\epsilon_1)}{m_1} - \frac{D(\epsilon_2) f(\epsilon_2)}{m_2} \right] . \quad (7)$$

The dipole matrix element μ for direct transitions of holes is found by comparing with Kahn's theory[12] to be

$$|\mu|^2/3 = \tfrac{1}{2}(e/k)^2 . \quad (8)$$

The resulting absorption (e.g., curve 2 in Fig. 1) matches the result of Murzin.[13]

When inhomogeneously broadened two-level systems are strongly irradiated, the level populations of the systems near resonance change. In a steady-state situation (i.e., when transient effects are damped out) the absorption coefficient decreases with increasing intensity according to Eq. (1), with exponent $x = 0.5$. The saturation intensity I_s is given by

$$I_s = \frac{\eta c \epsilon_0 \hbar^2}{2 T_1 T_2 L |\mu|^2/3} , \quad (9)$$

where T_1 is the energy relaxation time of the two-level

systems. Thus, a measurement of the saturation intensity suffices to determine directly the product of energy and phase relaxation times.

The dynamical time constants can be determined separately using the experimental technique of dynamical spectral hole burning,[6] i.e., observing a laser-induced dip in the linear absorption spectrum α_0,[21]

$$\alpha(\omega) = \alpha_0(\omega) \left[1 - \frac{(\Delta\omega_0)^2 I}{\Delta\omega \, I_s} \frac{\Delta\omega + \Delta\omega_0}{4(\omega - \omega_1)^2 + (\Delta\omega + \Delta\omega_0)^2} \right] .$$

(10)

The dip is Lorentzian, with a width given by the sum of the natural linewidth $\Delta\omega_0 = 2/T_2$ and the power-broadened linewidth $\Delta\omega$,

$$\Delta\omega = \Delta\omega_0 (1 + I/I_s)^{1/2} .$$

(11)

Note that Eq. (10) does not include the coherent contribution[21] for reasons to be discussed in Sec. VI.

The energy and phase relaxation times in p-type Ge can be linked to the scattering of holes by acoustic phonons, nonpolar-optical phonons, neutral impurities, charged impurities, and also other holes. This is in contrast to the 10-μm region,[2,22] where only acoustic- and optical-phonon scattering are relevant. Since, in our case, hole-hole scattering plays a role, the energy-loss rate of a carrier can become negative,[23] and therefore the picture used in Ref. 2 of a relaxation cascade is meaningless. As a consequence, we extend the model by allowing additional relaxation paths to other levels (Fig. 3). A given two-level system is depopulated by the scattering rates γ_1 and γ_2, respectively, and filled from other levels by λ_1 and λ_2, respectively. We assume that the populations of the other levels are not noticeably changed by the radiation, and obtain[24]

$$T_1 = \tfrac{1}{2}(\gamma_1^{-1} + \gamma_2^{-1}) .$$

(12)

Both inelastic and inter-valence-band scattering contribute to γ_1 and γ_2, whereas elastic scattering within one band does not.

The phase relaxation is given by the sum of the scattering rates in the upper and lower levels, ζ_1 and ζ_2,[22]

$$T_2 = 2(\zeta_1 + \zeta_2)^{-1} ,$$

(13)

where ζ_i is the sum of elastic- and inelastic-scattering rates.

We now turn to a discussion of the applicable scattering processes.[25] Scattering of holes from acoustic and optical phonons has been treated by Kranzer.[26] Identical results were obtained by Conwell for intraband scattering.[27] In the case of optical-phonon scattering, only the annihilation of phonons applies because of the low carrier energies considered here. The phonon-scattering rates enter the calculation of both dynamical times of the model as they describe inelastic processes.

Scattering with neutral impurities has been calculated by Erginsoy for the case of a single band only,[28]

$$\gamma = \frac{20\hbar a_0 N_n}{m} ,$$

(14)

with effective mass m; N_n is the density of neutral impurities and a_0 is the effective Bohr radius of these impurities, expected to be 41.4 Å for a gallium impurity[29] (which implies an effective mass of the bound hole of $0.22 m_0$, after Bohr's formula). Although the calculation of Erginsoy is valid only for $ka_0 < 0.5$, and, hence, Eq. (14) overestimates the neutral-impurity scattering for optical transitions above 80 cm^{-1}, we apply Eq. (14) to describe four distinct channels of intra- and interband scattering by neutral impurities,

$$\gamma_{ij} = \frac{20\hbar a_0 N_n}{m_i (m_i/m_j)^{3/2}}$$

(15)

accounting, in this way, for the different densities of the final states in the other valence band.[30] This is justified because the scattering amplitude does not depend on the scattering angle for scattering with neutral impurities. A further modification of Eq. (15) may, however, arise from the fact that the exchange interaction for different kinds of holes is different compared to the case in which only one type of hole is present. Since neutral-impurity scattering is elastic, it contributes to T_1 only for the case of interband scattering.

The scattering of holes with ionized impurities has been treated for a germanium-type band structure by Bir.[31] His results resemble the well-known Brooks-Herring formula for intraband scattering.[30] They are, however, restricted to the domain where the Born approximation is valid, which means $(k/\beta)^2 \gg 1$, where β is the inverse screening length. Unfortunately, the Born approximation is not always valid in our case, since $(k/\beta)^2 \approx 2$ for an example at a carrier concentration of 4×10^{14} cm^{-3}, a temperature of 40 K, and a wave number $k = 7 \times 10^5$ cm^{-1} (corresponding to a transition frequency of 31.2 cm^{-1}).

Blatt has treated the scattering with ionized impurities by a partial-wave analysis, and his results indicate that the scattering cross sections are overestimated by the Brooks-Herring formula for the wave-vector region of interest.[32] To improve Bir's result, we multiply it by a correction factor obtained as the ratio of the cross section after Blatt (for the largest screening length given there) to that obtained from the Born approximation. This is reasonable since the results from the partial-wave analysis do not depend very much on the screening length at large screening lengths. Again, we have to take only the interband terms when calculating the energy relaxation time.

Hole-hole scattering is treated similarly to impurity scattering here, because the Born approximation fails even more for scattering from equally charged particles. An expression for the hole-hole scattering rate given by Yassievich[33] is valid only for carrier energies $\varepsilon \gg kT$, which is not fulfilled in our case. Therefore we use the cross section σ for the scattering by a repulsive potential from Blatt, and calculate the scattering rate for hole-hole scattering:

$$\gamma = \int_0^\infty \sigma(\Delta k) N(\Delta k) v(\Delta k) \, d\Delta k ,$$

(16)

where Δk is the difference in the k vector of two holes,

$N(\Delta k)\,d\,\Delta k$ is the density of carriers with a difference Δk in wave vector, and $v(\Delta k)$ is their relative speed. Since a hole can lose or gain energy by scattering with another hole, this mechanism influences both the phase and energy relaxation times. However, only a part, f, of the scattered holes will gain or lose enough energy to leave the resonance region. Hence only this part leads to a depopulation of the resonant states and influences the energy relaxation time.

Figure 4 shows the scattering times corresponding to the various processes as a function of temperature, for an acceptor density of $N_A = 4.4 \times 10^{14}$ cm^{-3} and $v = 43.3$ cm^{-1}. The deformation-potential constants were taken from Pozhela[34] to be 5.9 and 13 eV for acoustic- and optical-phonon scattering, respectively. The concentrations of free carriers and of charged and neutral acceptors are calculated according to Ref. 35. Figure 4 also shows the energy and phase relaxation times calculated from our model. It was assumed that every hole-hole scattering event leads to a depopulation of the two-level system, i.e., $f = 1$. The same was assumed for acoustic-phonon scattering.

The phase relaxation is dominated by the scattering of heavy holes with ionized impurities above 40 K (curve d in Fig. 4). Below this temperature, the light-hole-to-heavy-hole interband scattering from neutral impurities forces T_2 to decrease with temperature (curve c). The energy relaxation time is dominated by hole-hole scattering in the heavy-hole band up to high temperatures, where optical-phonon scattering becomes important (curve g).
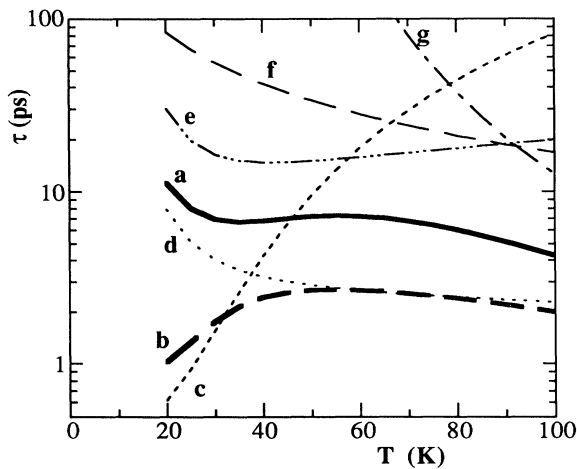
IV. SATURATION EXPERIMENT

The experimental setup [Fig. 5(a)] uses a pulsed, optically pumped far-infrared gas laser[8] with several hundred lines in the range 8–250 cm^{-1}, the strongest with pulse energies exceeding 10 mJ. As the typical pulse length is 100 ns [Fig. 5(c)], this corresponds to a power of 100 kW. The beam power is quantitatively varied over four orders of magnitude by a broadband precision attenuator.[36] Additionally, we used aluminized plastic foils with well-known transmittance, so that more than seven orders of magnitude of laser power are accessible.

The Ge samples with cross sections 8×8 mm^2 are mounted on a rectangular aperture (6×7 mm^2) in a helium-contact-gas cryostat. The sample thickness d is chosen to be 5 mm, so that $\alpha d \approx 1$. The samples are wedged with an angle of 2° to avoid standing-wave effects. For the same reason, the cryostat windows, consisting of 25- and 50-μm-thick Mylar foils, are tilted at 15° and 10°.

The radiation is focused on the sample with a paraboloidal mirror. A second paraboloid behind the cryostat collects the radiation transmitted through the sample and guides it via a second attenuator to a Golay detector. The second attenuator is operated to keep the pulse energy incident on the detector nearly constant, which eliminates nonlinearities of the detector. A beam splitter before the cryostat reflects a small portion of radiation to a second Golay detector. This signal serves as a reference to eliminate the variation of pulse energy from shot to shot (approximately 10%).

The measurement of transmittance is obtained by averaging over three pulses and switching five times between the sample and a reference sample made from an
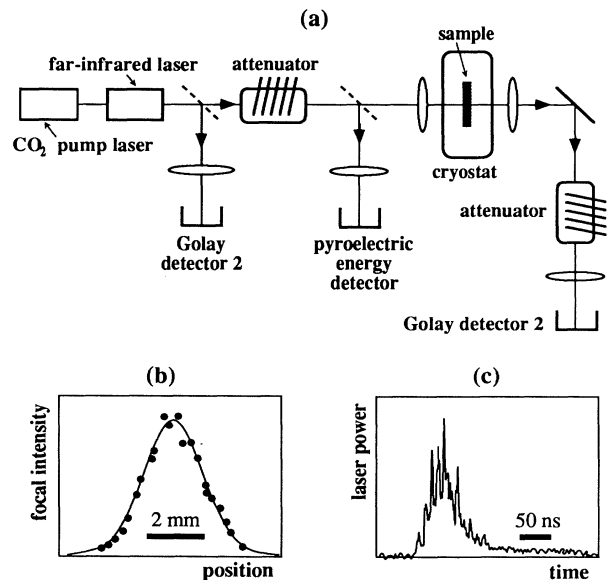

FIG. 4. Calculated relaxation times vs temperature, for $N_A = 4.4 \times 10^{14}$ cm^{-3} and $v = 43.3$ cm^{-1}. a, energy relaxation; b, phase relaxation; c, neutral-impurity interband scattering of light holes; d, ionized-impurity intraband scattering of heavy holes; e, hole-hole scattering of heavy holes; f, acoustic-phonon intraband scattering of heavy holes; g, nonpolar-optical-phonon intraband scattering of heavy holes.

FIG. 5. (a) Experimental setup to study the saturated absorption of p-type Ge; (b) typical cross-sectional intensity distribution at the sample location; (c) typical temporal structure of laser pulse.

undoped, ultrahigh-purity germanium sample of the same size. In this way we suppress effects of reflections and of the lattice absorption in determining the electronic absorption coefficient. The result of two measurements at different frequencies versus attenuation of laser power is shown in Fig. 6. The increase of transmittance with laser power is clearly visible.

Contrary to expectations from the model, the transmittance decreases at very high intensities (31.2-cm^{-1} data in Fig. 6). Since we observe, at maximum power, a reddish glow on the crystal surface, we ascribe the phenomenon to dielectric breakdown not to be followed in this context.

From the transmittance, we calculate the absorption coefficient $\alpha = -\ln(T)/d$. Fitting the absorption data with Eq. (1) ($x = 0.5$), and allowing for a residual, not intensity-dependent absorption, we derive both the saturation intensity and the small-signal absorption (Figs. 1 and 2). The residual absorption is evidently a Drude contribution.

To obtain the saturation intensity on an absolute scale, we measure the pulse energy of the radiation by directing it to an energy meter (see Fig. 5) placed at the appropriate distance to have the same attenuation through the air. The laser-pulse shape [Fig. 5(c)] is measured with a fast pyroelectric detector (response time 0.4 ns) connected to a digital oscilloscope (Hewlett Packard model 54111D). The spatial distribution of intensity [Fig. 5(b)] at the location of the sample is obtained by scanning a slit aperture across the beam. We find that the distribution follows a Gaussian beam profile with a waist radius on the order of 1 mm, both horizontally and vertically. From a separate measurement, we know the transmission of the cryostat windows. The reflectivity of the sample surface is calculated from the refractive index of germanium. With these data we are able to determine the intensity of the radiation in the Ge sample on an absolute scale.

At each attenuator setting, the absorption measurement represents an average over a span of intensities,
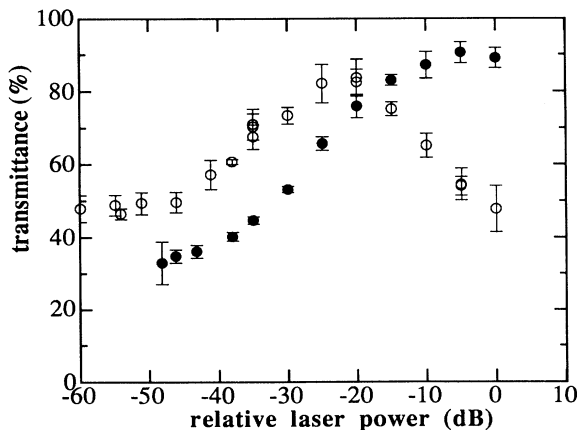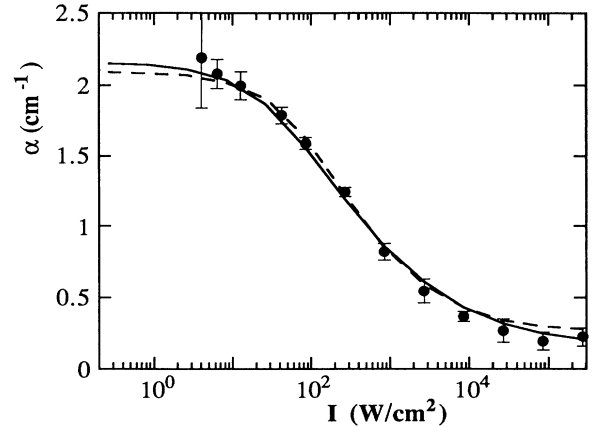

FIG. 7. Absorption coefficient α at $v = 111$ cm^{-1} vs intensity, with $N_A = 4.4 \times 10^{14}$ cm^{-3} at 40 K. The data are from the experiment Fig. 6. The curves represent a simulation of the nonlinear absorption according to inhomogeneous broadening (solid curve) and homogeneous broadening (dashed curve).

since the intensity varies in time and space. To correct for this, we numerically simulate the transmission through our sample with an intensity-dependent absorption coefficient corresponding to inhomogeneous broadening, with the saturation intensity as an open parameter. We take into account the temporal and spatial variation of intensity in the incident beam, as well as the variation due to absorption along the beam. The result is iteratively compared to the experimental saturation curve and finally yields a value for the saturation intensity. In Fig. 7 we see that we achieve excellent agreement between the theoretical model and measured data.

We also simulated the nonlinear transmission for the case of homogeneous broadening [Eq. (1), $x = 1$], as shown by a dashed curve in Fig. 7. This curve also describes the experimental data quite well, so that it seems impossible to decide between the two models from the intensity dependence of the absorption.

V. RESULTS AND DISCUSSION

The saturation intensity I_s was measured for several frequencies between 30 and 174 cm^{-1} in the temperature range 20–100 K. The range of measurement is limited to lower temperatures by the requirement that the laser pulse does not heat the sample by more than 3 K and that no other absorption mechanism obscures the intervalence-band absorption. The limit to higher temperatures is due to a decreasing small-signal absorption and an increasing saturation intensity. The resulting values of I_s are shown as data points in Figs. 8, 10, and 11–13. We mentioned before that the measurement of I_s suffices to determine directly $T_1 T_2$ through Eq. (9). Therefore, we have added a second vertical scale in Figs. 8, 10, and 11–13 that allows one to read the geometric mean value of T_1 and T_2.

FIG. 6. Transmittance vs power of p-type Ge sample with $N_A = 4.4 \times 10^{14}$ cm^{-3} at 40 K. Open circles, $v = 31.2$ cm^{-1}; solid circles, $v = 111$ cm^{-1}.

Figure 8 shows the results for a frequency of 43.3 cm^{-1}. We see that $T_1 T_2$ has a maximum at about 30 K. Also shown in Fig. 8 is a theoretical curve (a) calculated according to the model presented in Sec. III. Curve a corresponds to the curves for T_1 and T_2 shown in Fig. 4. The agreement between experimental and calculated data is good at high temperatures, but at low temperatures the calculated saturation intensity exceeds the measured value by an order of magnitude.

This discrepancy (which also exists in the results at other frequencies) leads us to reconsider the theoretical scattering rates of our model in Sec. III, for three different processes. First, we consider the efficiency of hole-hole scattering. If we choose the factor f to be 0.1 instead of 1 as in Sec. III, i.e., we assume that only every tenth hole scattering event leads to a depletion of the two-level system, the agreement between theory and experiment is improved in curve b in Fig. 8. Now the energy relaxation time is dominated over the whole temperature range by acoustic-phonon scattering. This leads to an increase of $T_1 T_2$ with decreasing temperature until T_2 drops down, so that a maximum evolves.

The neutral-impurity scattering seems overestimated at low temperatures. Since our theoretical calculations concerning this scattering mechanism in Sec. III were on weak grounds anyway, since they extrapolated from a one-band model, we modify our results. To obtain better agreement with the experimental data, we assume that the interband scattering from the light- to the heavy-hole band is only 25% of the calculated rate, and that the scattering from the heavy- to the light-hole band is twice the intraband scattering of the heavy holes. The first correction leads to an increase of T_2 and the latter to a decrease of T_1 at low temperatures. As a consequence, the maximum of $T_1 T_2$ shifts towards lower temperatures without changing the results at higher temperatures (curve c in Fig. 8).

Above 70 K there is still a slight disagreement between experiment and theory. Since the value of the optical deformation is uncertain anyway, we choose it to be slightly higher than in Ref. 34, namely $E_{op} = 21$ eV, and end up with the solid line (d) in Fig. 8, which now describes the data fairly well over the whole temperature interval. In Fig. 9 we present the modified curves of energy and phase relaxation times and the modified scattering times as they result from our calculations, to be compared with the unmodified ones in Fig. 4.

In Fig. 10(a), we have plotted our results for a frequency of 174 cm^{-1}. The theoretical curve is calculated with the same parameters as for 43.3 cm^{-1} and gives perfect agreement. Figure 10(b) gives the results at a frequency of 111 cm^{-1}. Here we find agreement between calculated and measured values above 50 K only. The disagreement below 50 K may come from a superposition of acceptor ionization, which contributes a significant part to the absorption in this range [Fig. 2(b)]. At 20 K, for example, the small-signal absorption by ionization is approximately double that of inter-valence-band excitation. The saturation behavior of acceptor ionization has been established separately[37,38] to be of homogeneously broadened, two-level character, with $I_s \approx 300$ W/cm^2 at 8 K. At lower doping, the relative influence of the ionizing transitions must decrease since the ionization degree increases. To observe this effect, we studied the saturation with two different samples, the doping of which was determined from room-temperature conductivity measurements.[39] In fact, the agreement between theory and experiment seems slightly better for the lower-doped sample. (Figure 11 shows results for a frequency of 111 cm^{-1}.)

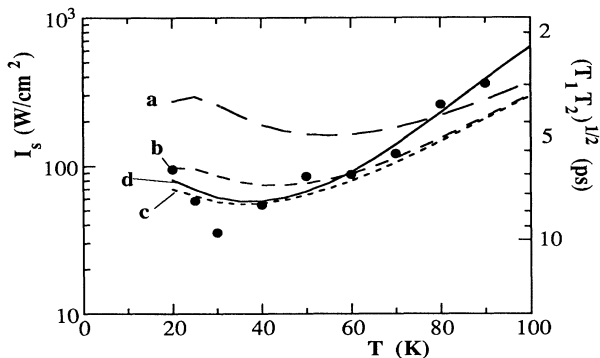Figure 12 displays our experimental and theoretical re-

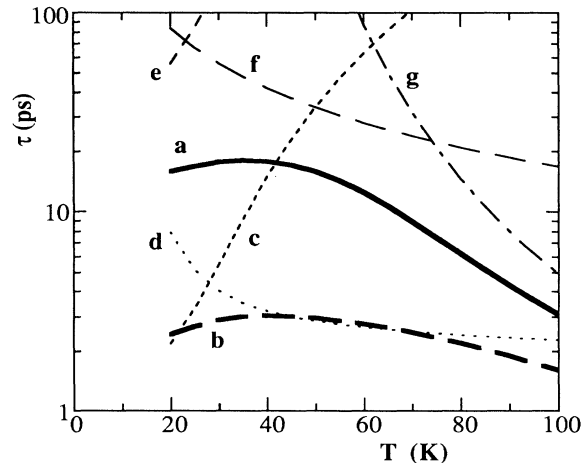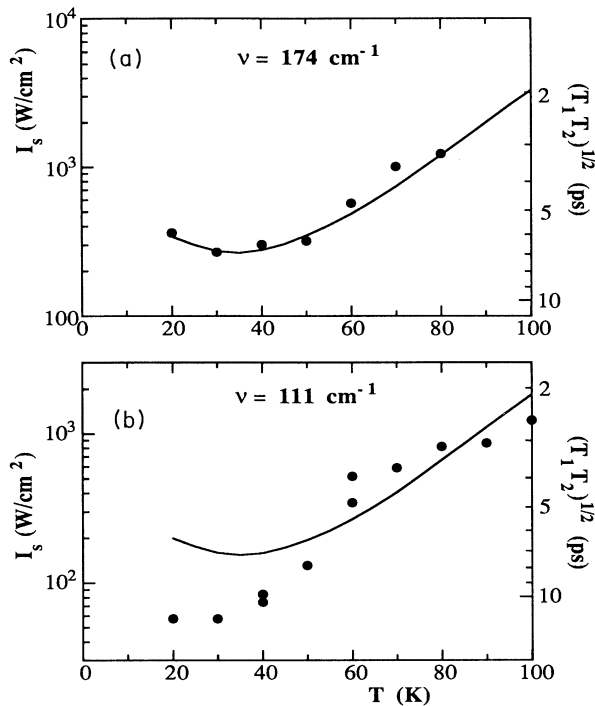FIG. 8. Saturation intensity (left-hand scale) and geometric mean of energy and phase relaxation times (right-hand scale) vs temperature, for $N_A = 4.4 \times 10^{14}$ cm^{-3} and $\nu = 43.3$ cm^{-1}. The circles are experimental data. The lines represent calculations according to the model of inhomogeneously broadened two-level systems (see text).

FIG. 9. Calculated relaxation times vs temperature for $N_A = 4.4 \times 10^{14}$ cm^{-3} and $\nu = 43.3$ cm^{-1}. a, energy relaxation time; b, phase relaxation time; c, neutral-impurity interband scattering of light holes; d, ionized-impurity intraband scattering of heavy holes; e, neutral-impurity interband scattering of heavy holes; f, acoustic-phonon intraband scattering of heavy holes; g, nonpolar-optical-phonon intraband scattering of heavy holes.
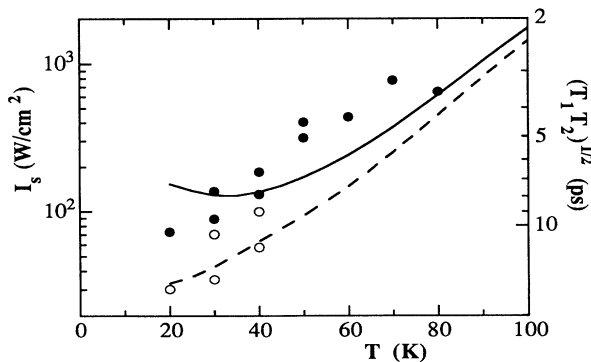
FIG. 10. Saturation intensity (left-hand scale) and geometric mean of energy and phase relaxation times (right-hand scale) vs temperature, for $N_A = 4.4 \times 10^{14}$ cm^{-3}. The circles are experimental data; the lines are from theory.

sults of the saturation intensity as a function of frequency. The saturation intensity [Fig. 12(a)] increases nearly linearly with frequency. The product of energy and phase relaxation time is, however, approximately independent of frequency [Fig. 12(b)], since it is related to I_s through the factor $|\mu|^2$ [Eq. (9)], which is inversely

FIG. 11. Saturation intensity (left-hand scale) and geometric mean of energy and phase relaxation times (right-hand scale) vs temperature at $\nu = 111$ cm^{-1}. Solid circles and solid line, $N_A = 3.7 \times 10^{14}$ cm^{-3}; open circles and dashed line, $N_A = 1 \times 10^{14}$ cm^{-3}. The lines are from theory.

proportional to frequency [Eq. (8)].

As we have seen before, the model of inhomogeneously broadened two-level systems is very well suited to describe the experimental data, even though it is only an approximation, because we have neglected any heating of the hole gas that would influence the different scattering rates. The opposite approach has been taken by Beregulin et al.[11] They investigated the bleaching of the intervalence-band absorption in p-type Ge at liquid-nitrogen temperature for the doping range 3×10^{14} to 5×10^{16} cm^{-3}. Because they were not able to explain their data in a model in which the only relevant relaxation process is acoustic-phonon scattering,[40] they assume that only the heating of the electron gas is responsible for the bleaching of the absorption. The basis for this is the assumption that hole-hole scattering is so fast that the holes are always distributed according to a Boltzmann function with a hole temperature T_h. In their model, T_h is calculated by equating the power absorbed by the electron gas to the power the electron gas loses to optical and acoustic phonons. Having T_h as a function of intensity, one can
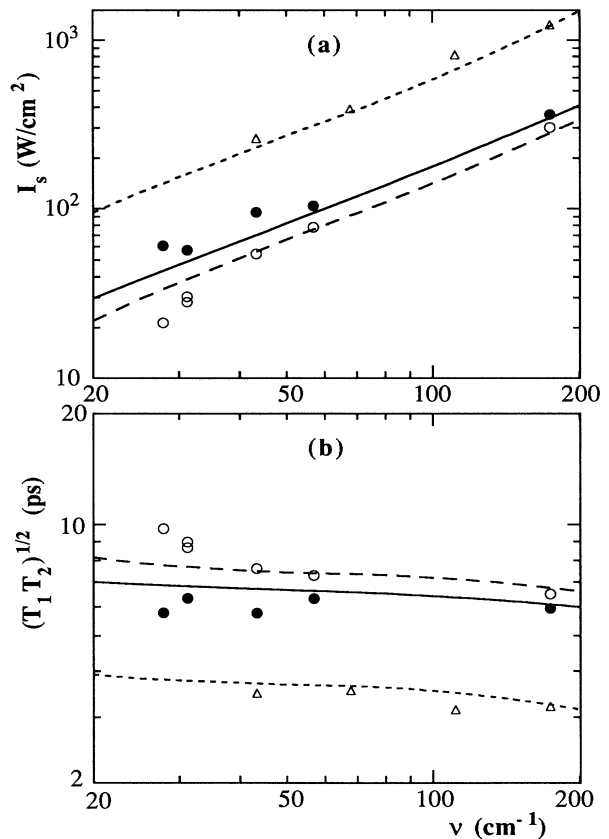

FIG. 12. (a) Saturation intensity and (b) geometric mean of energy and phase relaxation times, vs frequency for $N_A = 4.4 \times 10^{14}$ cm^{-3}. The points are from the experiment; the curves represent theory. Solid line and solid circles, 20 K; dashed line and open circles, 40 K; dotted line and open triangles, 80 K.
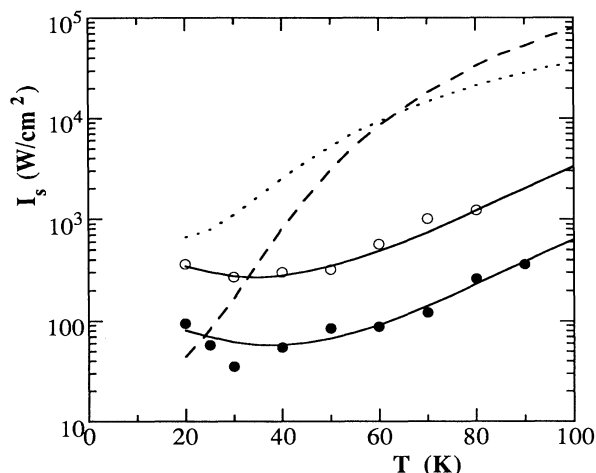
FIG. 13. Saturation intensity vs temperature for $N_A = 4.4 \times 10^{14}$ cm^{-3}. The results of the model according to Beregulin (Ref. 11) for 43.3 cm^{-1} (dashed line) and 174 cm^{-1} (dotted line) are compared to our experimental data given by solid (43.3 cm^{-1}) and open (174 cm^{-1}) circles. The solid lines represent the results of the model of inhomogeneously broadened two-level systems [Figs. 8 and 10(a)].

FIG. 14. Setup for far-infrared hole-burning experiment.

calculate the absorption as a function of intensity, which results in curves similar to those in Fig. 7. We have repeated these calculations and then have fitted the results to Eq. (1), with $x = 0.5$, to obtain a comparison to our theory. The result is shown in Fig. 13. Clearly, the heating model is not able to describe the data observed by us. The discrepancy cannot be removed by varying the optical and acoustic deformation constants, even by large factors. In their work Beregulin et al.[11] also present experimental data of saturated absorption. For a doping level comparable to ours and a temperature of 78 K, they obtain a saturation intensity [using Eq. (1), with $x = 1$] of 8 kW/cm^2 at a frequency of 111 cm^{-1}. To compare this value to our analysis ($x = 0.5$), we must divide their result by a factor of approximately 3 and obtain $I_s \approx 3$ kW/cm^2, which is of the same order of magnitude as our result [e.g., Fig. 12(a)].

VI. HOLE-BURNING EXPERIMENT

Theory predicts that the absorption saturation leads to a laser-induced spectral dip ("dynamical hole burning") for the case of inhomogeneously broadened, two-level systems (Sec. III). This effect is often applied in spectroscopy to reveal the homogeneous linewidth of inhomogeneously broadened resonances. The experiment exposes the sample to strong radiation at a frequency ω_1 to change the population of systems near resonance. This change in detected by the measurement of the absorption spectrum with a weak source [Eq. (10)].

Figure 14 shows the setup for our pump-and-probe experiment. The strong source, labeled 1, is the laser al-
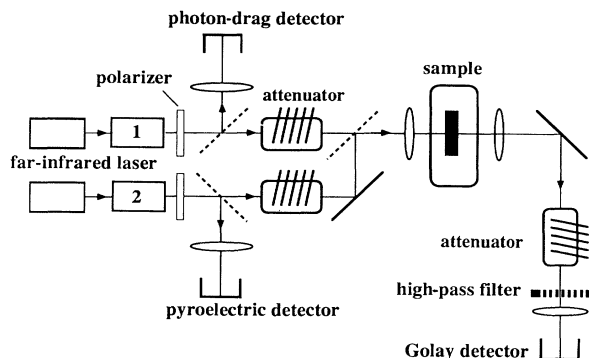
ready described before. The probe laser labeled 2 is a similar, optically pumped far-infrared gas laser with a shorter length. It operates on the same lines, but has a smaller pulse energy. In the experiment both laser beams are linearly polarized in the same direction by free-standing wire grids. The pulse shapes are monitored during the experiment with photon-drag and fast pyroelectric detectors, so that we can control the temporal overlap. Only pulses with an optimal overlap are selected for the measurement.

The attenuated probe beam is coupled into the path of the pump beam with a Mylar beam splitter. A high-pass filter in front the Golay cell blocks the pump beam so only the probe pulse reaches the detector. We use a cutoff-waveguide filter consisting of a metal plate with cylindrical holes.[41] It is chosen to have a transmittance of $\geq 20\%$ above 40 cm^{-1}, but to suppress radiation below 33 cm^{-1} by more than nine orders of magnitude. The frequency of the pump laser is chosen to be 31.2 cm^{-1}. By this arrangement, we are limited to measure the high-

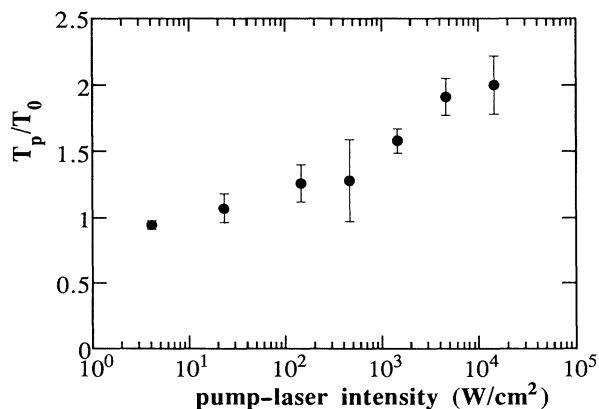FIG. 15. Normalized transmittance of a weak probe pulse at 45.3 cm^{-1} as a function of the intensity of the pump laser at 31.2 cm^{-1}, for $N_A = 3.7 \times 10^{14}$ cm^{-3} at 40 K.

frequency side of the saturation dip. In the measurement we take the ratio T_p/T_0 of the probe-laser signal with the saturating beam on and off. As an example, the results for a probe frequency of 45.3 cm^{-1} are shown in Fig. 15. The effect of saturation is clearly evident. The saturation curves are recorded for four frequencies, and are further evaluated to yield absorption spectra. Great difficulty arises from the incomplete temporal overlap of both laser pulses, which results in large error bars. The spectra in Fig. 16 have the pump intensity as a parameter, and the absorption coefficient is normalized to the small-signal absorption. The data points at the pump frequency 31.2 cm^{-1} are taken from the one-laser saturation experiment (Sec. IV) that yields a saturation intensity $I_s = 30$ W/cm^2 (Fig. 12).

Inspection of the data points in Fig. 16 indeed reveals a diplike structure. This dip strongly broadens with increasing pump-laser intensity, as is expected from power broadening in the model of inhomogeneously broadened two-level systems. For a quantitative comparison, we fit the theory [Eq. (10)] to the entity of data points in Fig. 16 and obtain the set of theory curves in Fig. 16, with the homogeneous linewidth as the sole fitting parameter, resulting in $\Delta\nu_0 = 23$ cm^{-1} [full width at half maximum (FWHM)]. This corresponds [Eq. (4)] to a phase relaxation time $T_2 = 0.5$ ps. Inspection of Fig. 16 reveals that the curves may well describe the high-intensity data, but systematically yield overly large dip widths for the low- and medium-intensity points. We take this as an indication that we have an additional nonlinearity at the highest powers, most probably an increase of carrier scattering due to an overall heating of the carriers. Since we are interested in the carrier dynamics at negligible heating, we have performed the fit to the low-intensity spectra alone. The result is an approximately threefold narrower dip width of 7 cm^{-1}, yielding $T_2 = 1.4$ and 1.6 ps, respectively for the 15- and 150-W/cm^2 data.

In our model (Sec. III), we have left out the term describing a coherent dip that should be superimposed with a linewidth $\Delta\omega_{coh} = 2/T_1$.[21,7] The reason is that the coherent dip is too narrow to be resolved with our present technique: When we take the experimental value $I_s = 30$ W/cm^2 equivalent to $(T_1T_2)^{1/2} = 9$ ps (Fig. 12), and use $T_2 = 1.5$ ps, we obtain $T_1 = 43$ ps and, hence, $\Delta\nu_{coh} = 0.5$ cm^{-1} (FWHM). Note that the data at 31.2 cm^{-1} result from a one-laser experiment in which no coherent contribution exists. Therefore, the hole-burning experiment cannot independently determine both time constants T_1 and T_2, as was possible with the experiments at 1000 cm^{-1} where the relaxation is much faster.[7]

The observed dip width of about 7 cm^{-1} (FWHM) is not much smaller than the saturating laser's frequency of 31.2 cm^{-1}, as is assumed in the theoretical derivation of Eq. (10). This adds to the uncertainty given by the scarce
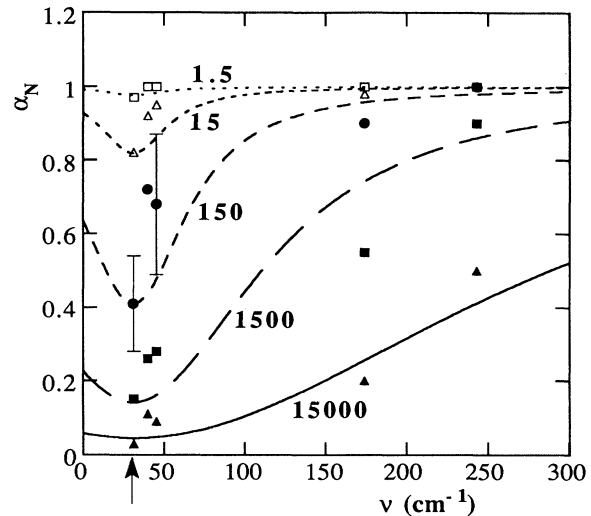

FIG. 16. Normalized probe absorption in hole-burning experiment at 40 K. The frequency of the pump laser is marked by an arrow. The lines represent a fit according to the model of inhomogeneously broadened two-level systems [Eq. (10)] to the entirety of data shown. The pump intensity increases from 1.5 W/cm^2 (uppermost curve and data points) in decade steps up to 15 kW/cm^2.

data of the dip experiment (Fig. 16) in the determination of $T_2 \approx 1.5$ ps. Notwithstanding, the dip data of $T_2 = 1.5$ ps and $T_1 = 43$ ps agree favorably with the results of Sec. V, as displayed in Fig. 9, where we obtain 2.9 and 20 ps, respectively.

VII. CONCLUSIONS

We have shown that the model of inhomogenously broadened two-level systems describes very well the saturation behavior of the inter-valence-band absorption, over a wide span of temperatures and far-infrared frequencies. The agreement is surprising in view of the simplicity of the model. The corrections introduced in the theoretical treatment of low-energy carrier scattering are rather convincing, because all measurements can be described with the same set of parameters, and may therefore stimulate further theoretical work. The alternative model of optical heating[11] is far from describing the experimental data; it obviously overestimates hole-hole scattering.

ACKNOWLEDGMENTS

[1]A. F. Gibson, C. A. Rosito, C. A. Raffo, and M. F. Kimmit, Appl. Phys. Lett. **21**, 356 (1972).

[2]F. Keilmann, IEEE J. Quantum Electron. **QE-12**, 592 (1976).

[3]C. R. Phipps, Jr. and S. J. Thomas, Opt. Lett. **1**, 93 (1977).

[4]E. V. Beregulin, P. M. Valov, and I. D. Yaroshetskii, Fiz. Tekh. Poluprovodn. **12**, 239 (1978) [Sov. Phys.—Semicond. **12**, 138 (1978)].

[5]R. B. James and D. L. Smith, Phys. Rev. B **21**, 3502 (1980).

[6]*High Resolution Laser Spectroscopy,* edited by K. Shimoda, Topics in Applied Physics Vol. 13 (Springer-Verlag, Berlin, 1976).

[7]F. Keilmann, Appl. Phys. **14**, 29 (1977).

[8]C. T. Gross, J. Kiess, A. Meyer, and F. Keilmann, IEEE J. Quantum Electron. **QE-23**, 377 (1987).

[9]A. A. Andronov, Int. J. Infrared Millimeter Waves **16**, 149 (1986).

[10]S. Komiyama and S. Kuroda, Jpn. J. Appl. Phys. **26**, L71 (1987).

[11]E. V. Beregulin, S. D. Ganichev, K. Yu. Glukh, and I. D. Yaroshetskii, Fiz. Tekh. Poluprovodn. **21**, 1005 (1987) [Sov. Phys.—Semicond. **21**, 615 (1987)].

[12]A. H. Kahn, Phys. Rev. **97**, 1647 (1954).

[13]V. N. Murzin, Fiz. Tekh. Poluprovodn. **7**, 1610 (1973) [Sov. Phys.—Semicond. **7**, 1074 (1974)].

[14]Yu. T. Rebane, Fiz. Tekh. Poluprovodn. **14**, 289 (1980) [Sov. Phys.—Semicond. **14**, 169 (1980)].

[15]F. Seitz, *Modern Theory of Solids* (McGraw-Hill, New York, 1940).

[16]R. L. Jones and P. Fisher, J. Phys. Chem. Solids **26**, 1125 (1965).

[17]G. E. Stillman, C. M. Wolfe, and J. O. Dimmock, in *Semiconductors and Semimetals,* edited by R. K. Willardson and A. C. Beer (Academic, New York, 1977), Vol. 12.

[18]M. Ikezawa and T. Nanba, J. Phys. Soc. Jpn. **45**, 148 (1978).

[19]R. Brazis and F. Keilmann, Solid State Commun. **70**, 1109 (1989).

[20]R. H. Pantell and H. E. Puthoff, *Fundamentals in Quantum Electronics* (Wiley, New York, 1969).

[21]M. Sargent III, Appl. Phys. **11**, 107 (1976).

[22]M. Sargent III, Opt. Commun. **20**, 298 (1977).

[23]C. J. Hearn, Proc. Phys. Soc. London **86**, 881 (1965).

[24]W. Demtröder, *Laser Spectroscopy* (Springer-Verlag, Berlin, 1982).

[25]For a recent review, see C. Jacoboni and L. Reggiani, Rev. Mod. Phys. **55**, 645 (1983).

[26]D. Kranzer, Phys. Status Solidi A **26**, 11 (1974).

[27]E. M. Conwell, in *Solid State Physics,* edited by F. Seitz, D. Turnbull, and H. Ehrenreich (Academic, New York, 1967), Suppl. 9.

[28]C. Erginsoy, Phys. Rev. **79**, 1013 (1950).

[29]E. Otsuka, K. Murase, and J. Iseki, J. Phys. Soc. Jpn. **21**, 1104 (1966).

[30]H. Brooks, *Advances in Electronics and Electron Physics* (Academic, New York, 1955), Vol. 7.

[31]G. I. Bir, E. Normantas, and G. E. Pikus, Fiz. Tverd. Tela (Leningrad) **4**, 1180 (1962) [Sov. Phys.—Solid State **4**, 867 (1962)].

[32]F. J. Blatt, J. Phys. Chem. Solids **1**, 262 (1957).

[33]I. N. Yassievich and I. D. Yaroshetskii, Fiz. Tekh. Poluprovodn. **9**, 857 (1975) [Sov. Phys.—Semicond. **9**, 565 (1975)].

[34]Yu. Pozhela and A. Reklaitis, Fiz. Tekh. Poluprovodn. **11**, 709 (1977) [Sov. Phys.—Semicond. **11**, 414 (1977)].

[35]J. S. Blakemore, *Semiconductor Statistics* (Pergamon, Oxford, 1962).

[36]F. Keilmann, Proc. SPIE **666**, 213 (1986).

[37]T. Theiler, doctoral thesis, Universität Stuttgart (unpublished), 1989.

[38]T. Theiler, H. Navarro, R. Till, and F. Keilman (unpublished).

[39]S. M. Sze and J. C. Irvin, Solid State Electron. **11**, 599 (1968).

[40]D. A. Parshin and A. R. Shabaev, Zh. Eksp. Teor. Fiz. **92**, 1471 (1987) [Sov. Phys.—JETP **65**, 827 (1987)].

[41]F. Keilmann, Int. J. Infrared Millimeter Waves **2**, 259 (1981).